Journal of Innovative Optical Health Sciences
Vol. 2, No. 4 (2009) 375–385

World Scientific
www.worldscientific.com

QUANTITATIVE REDOX SCANNING OF TISSUE SAMPLES USING A CALIBRATION PROCEDURE

HE N. XU*, BAOHUA WU*,†, SHOKO NIOKA†, BRITTON CHANCE†,
and LIN Z. LI*,‡

*Molecular Imaging Laboratory, Department of Radiology
University of Pennsylvania, Philadelphia PA 19104, USA

†Johnson Research Foundation
Department of Biochemistry and Biophysics
University of Pennsylvania, PA 19104, USA

‡linli@mail.med.upenn.edu

The fluorescence properties of reduced nicotinamide adenine dinucleotide (NADH) and oxidized flavoproteins (Fp) including flavin adenine dinucleotide (FAD) in the respiratory chain are sensitive indicators of intracellular metabolic states and have been applied to the studies of mitochondrial function with energy-linked processes. The redox scanner, a three-dimensional (3D) low temperature imager previously developed by Chance *et al.*, measures the *in vivo* metabolic properties of tissue samples by acquiring fluorescence images of NADH and Fp. The redox ratios, i.e. Fp/(Fp+NADH) and NADH/(Fp+NADH), provided a sensitive index of the mitochondrial redox state and were determined based on relative signal intensity ratios. Here we report the further development of the redox scanning technique by using a calibration method to quantify the nominal concentration of the fluorophores in tissues. The redox scanner exhibited very good linear response in the range of NADH concentration between 165–1318 μM and Fp between 90–720 μM using snap-frozen solution standards. Tissue samples such as human tumor mouse xenografts and various mouse organs were redox-scanned together with adjacent NADH and Fp standards of known concentration at liquid nitrogen temperature. The nominal NADH and Fp concentrations as well as the redox ratios in the tissue samples were quantified by normalizing the tissue NADH and Fp fluorescence signal to that of the snap-frozen solution standards. This calibration procedure allows comparing redox images obtained at different time, independent of instrument settings. The quantitative multi-slice redox images revealed heterogeneity in mitochondrial redox state in the tissues.

Keywords: NADH; flavoprotein; redox ratio; mitochondria; tissue heterogeneity.

1. Introduction

Mitochondrion plays key roles in many biological processes including metabolism, biosynthesis, signaling, and apoptosis.[1] Energy-carrying coenzymes, reduced nicotinamide adenine dinucleotide (NADH) and reduced flavin adenine dinucleotide ($FADH_2$) are fed into the electron transport chain in mitochondrial inner membrane for ATP synthesis by oxidative phosphorylation.[2] In 1950s, Chance *et al.* first correlated the mitochondrial metabolic state

‡Corresponding author.

to oxidation-reduction levels of respiratory coenzymes in the electron transport chain.[3] Later on he and other investigators employed the fluorescence of NADH and oxidized flavoprotein (Fp) including FAD to study the mitochondrial metabolic state. Seminated from Chance's pioneering work, cellular NADH and/or Fp fluorescence has been widely used for probing cellular metabolism, proliferation, differentiation, transformation, and treatment response.[4–10] The NADH fluorescence measurement has already been applied to patients.[7,11] Chance *et al.* also established that the fluorescence ratio of NADH and Fp can provide a sensitive indicator of mitochondrial redox state.[12–16] A highly active mitochondrial metabolic state would result in less NADH (lower NADH redox potential), more Fp, and higher Fp redox ratio Fp/(NADH + Fp). Current biomedical research has shown that mitochondrial redox state is a key mediator for many biological processes including metabolism, apoptosis, and signaling events.[17] The abnormalities in mitochondrial redox states have been associated with diseases such as diabetes[18,19] and cancer metastatic potential.[20–22] Thus, the measurement of the *in vivo* mitochondrial redox state in tissue has a great significance for biomedical research and clinical practice.

In late 1970s, redox scanning has been developed by Quistorff and Chance *et al.* to image the mitochondrial redox state in tissue *ex vivo*.[23–26] Redox scanning obtains high-resolution three-dimensional (3D) maps of mitochondrial redox state in tissue samples by measuring the fluorescence of NADH and Fp in snap-frozen biological samples. This method has several advantages: (1) imaging the *in vivo* metabolic states in live biological tissues can be achieved by a snap-freezing procedure in liquid nitrogen. Snap-freeze prevents the NADH and Fp signal from changing within a minute once the tissue is physiologically perturbed; (2) the measurement of redox ratio, i.e. Fp/(Fp + NADH) or NADH/(Fp + NADH) has the advantages of being independent of mitochondrial density, avoiding interference from other fluorophores, and demanding less stringent instrumentation. The ratio method may also compensate the influence of blood absorption;[23] (3) The fluorescence of NADH and Fp under the low temperature of liquid nitrogen are about 10-fold enhanced compared to that under room temperature;[23] (4) Multi-slice redox scanning images have a high in-plane resolution of 40–100 μm, much better than other *in vivo* fluorescence imaging methods (∼mm). Recently, CCD-based redox imaging has been developed to acquire the redox state of mouse colons *in vivo* under room temperature.[27]

The redox ratios, i.e. Fp/(Fp + NADH) and NADH/(Fp+NADH) obtained from previous redox imaging method were based on relative signal intensities of the intrinsic NADH and Fp fluorescence. Since the signal intensities depend on the instrument settings such as filters, fiber-optical probe, photon multiplier tube (PMT) dynamic range, and mercury lamp condition, it is difficult to compare images obtained from different time and/or with different instrument.

The goal of this investigation is three-fold: (1) to establish the linear dynamic range of the redox scanner by using snap-frozen solution standards at various concentrations; (2) to quantify the nominal concentration of NADH and Fp in snap-frozen tissue by scanning the tissue sample together with the snap-frozen standards adjacently placed; (3) to obtain the *in vivo* mitochondrial redox states of tissue quantitatively based on concentration ratios of the fluorophores. The nominal concentration and quantitation of mitochondrial redox states in tissue determined by using the developed calibration procedure in this study facilitates the comparison of the redox ratio images obtained at different time or with different instrument settings. A part of this work has been preliminarily reported in a preprint published in the Proceedings of SPIE, 2009.[28]

2. Materials and Methods

2.1. *Preparation of NADH and FAD solution standards*

To establish the calibration curves of NADH (Nicotinamide adenine dinucleotide, reduced disodium salt) and FAD (Riboflavin 5′-adenosine diphosphate disodium salt), two sets of solution standards were prepared by weighing out the appropriate amount of NADH and FAD (in powder form) purchased from Sigma-Aldrich (St. Louis, Missouri). NADH and Fp powder were diluted with 10 mM Tris-HCl buffer with pH = 8.0 and Hanks balanced salt solution, respectively. The NADH stock solution concentration was determined to be 1,318 μM by a UV-Vis spectrometer with $\varepsilon = 6,220\,\mathrm{M}^{-1}\,\mathrm{cm}^{-1}$ at 360 nm and the FAD stock solution concentration was 719 μM

using $\varepsilon = 11{,}300\,\mathrm{M}^{-1}\,\mathrm{cm}^{-1}$ at 450 nm[4] (see also the product data sheet from Sigma-Aldrich). Four solutions at various concentrations of NADH or FAD were prepared by serial dilution and separately injected into 1/8" Teflon tubes of about 1 cm long with one sealed-end. All the tubes were mounted in play-dough at the bottom of a plastic screw closure of 2.4 cm in diameter and 1 cm in height before injection. Nine tubes containing NADH and FAD standards at various concentrations and a Tris-HCl buffer control forming a 3×3 matrix were placed in the closure. After injection of the standards, the plastic closure was snap-frozen by being fully dipped into liquid N_2. Relatively homogeneous freezing result was produced by this rapid freezing process. Mounting buffer composed of ethanol–glycerol–water (10:30:60, freezing point -30°C) chilled in liquid N_2 was then filled into the plastic closure to strengthen the standard matrix for the grinding process before scanning. The prepared sample was dipped into liquid N_2 for further consolidation and storage.

2.2. *Preparation of tissue samples with reference standards*

An animal protocol has been approved by the Institutional Animal Care and Use Committee at the University of Pennsylvania. The mice bearing human breast tumors (MCF-7) in their upper thigh of the hind legs were anesthetized and snap-frozen with liquid N_2. The snap-frozen technique ensures NADH, Fp, and the metabolic states in tumors were all maintained at their *in vivo* levels.[23] The frozen tumors were then quickly excised using a handsaw in a low temperature environment and kept in liquid nitrogen awaiting sample preparation and redox imaging. The mice for organ harvest were provided by Dr. Ben Stanger at the Department of Medicine in the University of Pennsylvania, School of Medicine. Mouse organs such as liver and spleen were harvested via proper open-chest surgical procedure. The organs were removed with a pair of scissors and dropped into liquid N_2 within 2 s for sample preparation and redox imaging.

To prepare a tissue sample with reference standards, mounting buffer was placed in a plastic closure and chilled with liquid nitrogen till the mounting buffer reached a workable firmness. A snap-frozen tissue sample (a tumor or a mouse organ) was carefully placed into the chilled mounting medium, followed by quickly inserting the reference tubes containing frozen standards (one NADH and one Fp with known concentration) into the mounting medium adjacently to the tissue sample. More chilled mounting buffer was added into the plastic closure to cover the sample and the reference tubes. The sample was then dipped into liquid nitrogen for consolidation and storage.

2.3. *Redox scanning of the standards and tissue samples*

Samples were imaged by the redox scanner (see Fig. 1 for the schematics) at the low temperature of liquid nitrogen as described previously.[23–25] Briefly, the sample surface was milled flat by the grinder equipped with the scanner under liquid nitrogen. A bifurcated fiber-optic probe transmits the excitation photons generated by a mercury arc lamp and collects the emission photons from samples. This probe was a bundle of five UV quartz fibers of 90 μm in diameter (Schott Inc., Elmsford, New York) transmitting excitation photons and one center quartz fiber of 50 μm in diameter (Polymicro Technologies, LLC, Phoenix, Arizona) with UV attenuation <0.1 dB/m transmitting the emission photons. The probe driven by x and y stepper motors scanned over the flat sample surface. The Fp excitation channel filter centers at 430 nm with a bandpass of 50 nm and the Fp emission filter centers at 525 nm with a bandpass of 64 nm; the NADH excitation channel filter centers at 360 nm with 52 nm bandpass and the emission filter at 430 nm with 50 nm bandpass. Proper neutral density filters were inserted to the emission channels

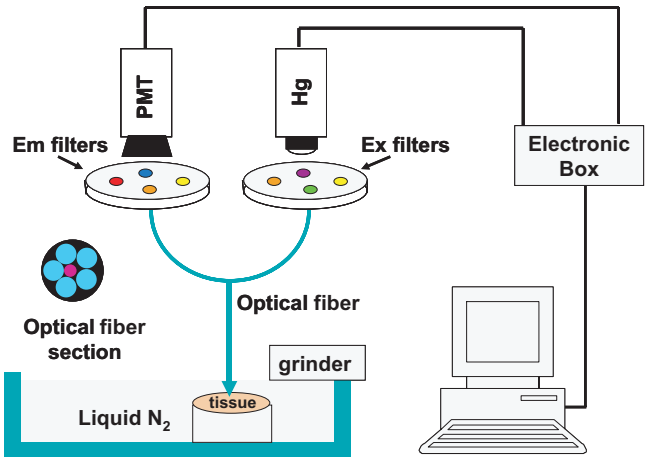

Fig. 1. Schematics of the redox scanner.

when the signal became saturated. The NADH and Fp emission signals were transmitted to the PMT as the fiber-optic probe scanned over the sample surface. The PMT used was an R928 from Hamamatsu Inc. with a sensitivity range of 185–900 nm. To prevent red light leakage, we added a short-pass glass filter (472 nm ± 168 nm with an out-of-band rejection of O.D. 4.5 for 640 nm or longer) in the NADH channel, which yields the total out-of-band rejection of O.D. 7.5 for red light. The collected signal was processed by a PC computer to construct the images of NADH and FAD solution standards and that of a tissue sample.

The scanning matrix for the solution standards was 64 × 64 with a step size of 200 μm. For tissue samples, the scanning matrix was either 64×64 with a step size of 200 μm or 128 × 128 with a step size of 100 μm.

2.4. *Data analysis*

The acquired images were analyzed to generate the mean value and the standard deviation using MatLab® software, with signal intensity corrected if neutral density filters were used. For solution standards, the area of each reference tube containing the standard at a specific concentration was selected as the region of interest (ROI). The mean value of the signal intensities from each standard's image was computed with the subtraction of the background signal of the blank control. The average signal intensity of NADH or Fp was plotted against the fluorophore concentrations. Linear regression was performed to obtain its slope and standard deviation. For tissue samples, ROIs were carefully drawn along the sample rim and the area of each reference tube adjacently placed. The nominal NADH and Fp concentrations in the tissue samples were obtained by comparing the tissue signal intensities with those of the reference standards.

Redox images are displayed with a color bar on the right side of each image indicating the range of data values. NADH or Fp images are in concentrations (μM), and redox ratio values are between 0 and 1. A histogram for a ROI in an image was generated by counting the number of pixels for each specific value of NADH or Fp concentration or redox ratio.

3. Results

3.1. *Calibration results*

Figures 2 and 3 show the calibration curves of fluorescence of NADH and FAD versus the concentrations of the fluorophores when the high voltage of PMT was set at 830 and 900 V, respectively. The concentration of NADH standards is 1318, 659, 329, and 165 μM, respectively. The concentration of FAD is 720, 359, 179, and 90 M, respectively. Linear regression shows that both curves have high linearity with the correlation coefficient $R^2 = 0.996$ and 0.94 for NADH and FAD, respectively, at 830 V and $R^2 = 0.99$ and 0.98 for NADH and FAD, respectively, at 900 V. The slope of NADH and FAD curve is 0.16 ± 0.01 and 0.05 ± 0.01, respectively, at 830 V, and 0.27 ± 0.01 and 0.07 ± 0.00, respectively, at 900 V. The ratio of NADH curve slope to that of FAD is 3.8 and 3.7 at 830 and 900 V, respectively, representing the signal strength ratio of NADH channel to Fp channel.

3.2. *Quantitative redox images of various tissue samples*

We have obtained quantitative redox images by using the reference standards for various biological

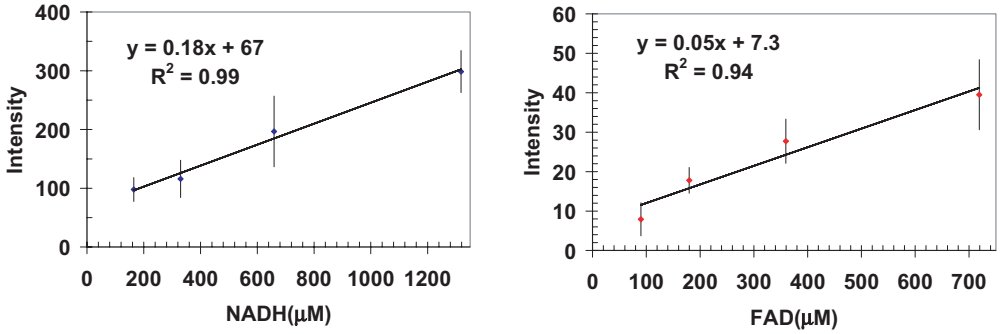

Fig. 2. Calibration curves of the snap-freeze solution standards obtained at 830 V of PMT voltage. Data were fit to a straight line by linear regression. The error bar represents the standard deviation of the fluorescence image at a specific concentration. The y-axis is the net signal intensity obtained by subtracting the signal intensity of buffer.

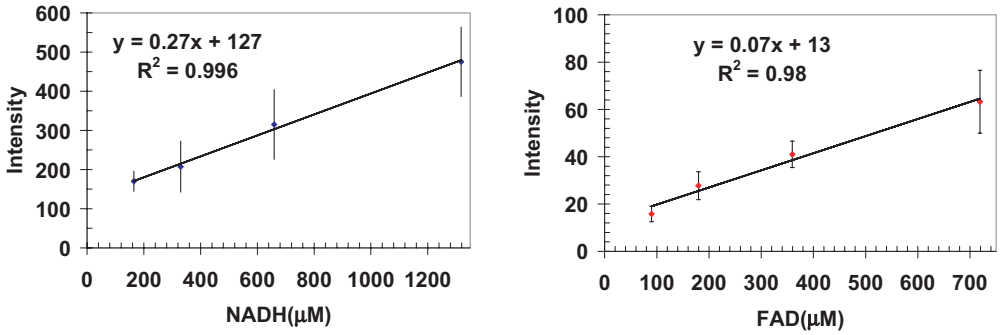

Fig. 3. Calibration curves of the snap-freeze solution standards obtained at 900 V of PMT voltage. Data were fit to a straight line by linear regression. The error bar represents the standard deviation of the fluorescence image at a specific concentration. The y-axis is the net signal intensity obtained by subtracting the signal intensity of buffer.

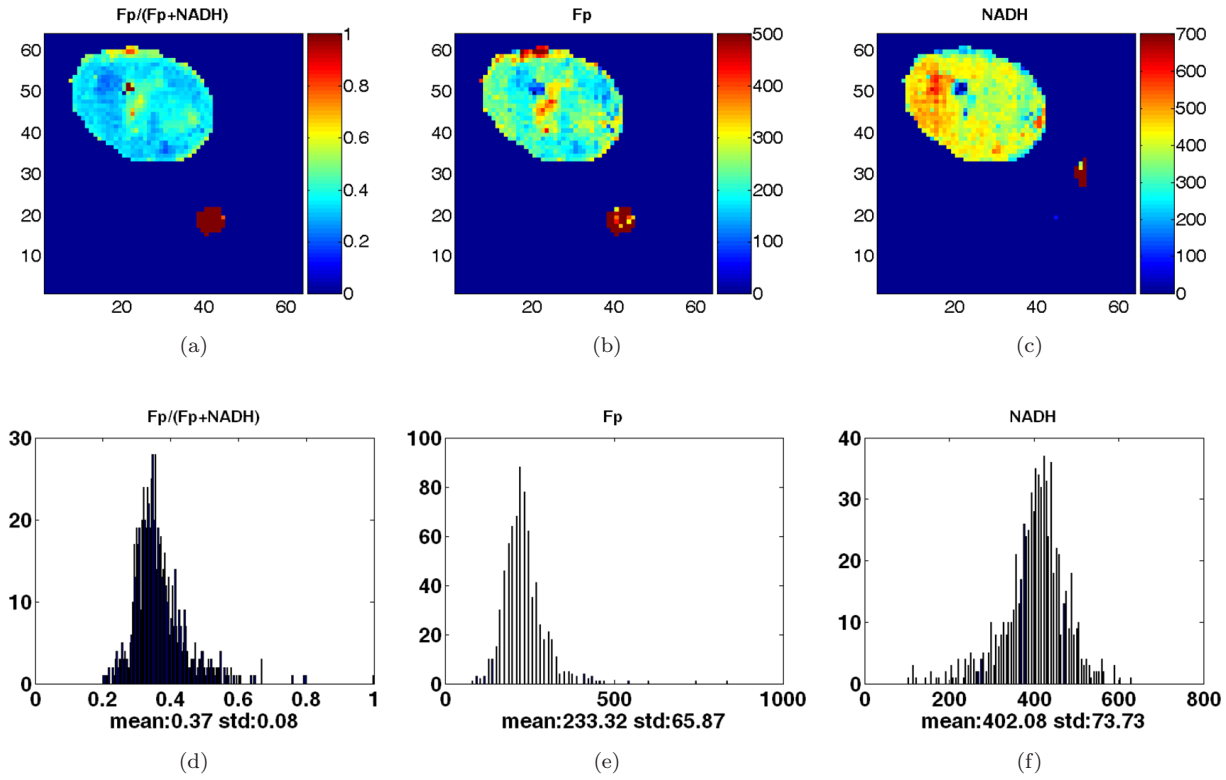

Fig. 4. Typical redox scanning images of a snap-frozen tumor from a mouse xenograft of human breast cancer cell line MCF-7. Matrix size: 64×64, in-plane resolution $200 \times 200\,\mu m^2$. NADH and Fp are displayed in concentrations (μM). The grinding depth of the tumor section was 1.4 mm from the tumor surface. The lower three graphs are the histograms of Fp redox ratio, Fp, and NADH nominal concentration in the tumor section, respectively. The dark red spots in the images of upper row are reference standards.

tissue samples. Typical redox scanning images of a snap-frozen tumor from a MCF-7 breast cancer mouse xenograft were given in Fig. 4, revealing some degree of heterogeneity. The depth of the tumor section was 1.4 mm from the tumor surface. The round spot outside the tumor area is the reference standard of NADH or FAD. As shown by the concentration color bar, the nominal concentration of NADH in the tumor was in the range of 200–600 μM and that of Fp was between 100 and 450 μM. The Fp redox ratio was between 0.2 and 0.6 with a full width at half maximum (FWHM) of $\sim$0.15. With a ROI drawn over the tumor area, we obtained mean NADH $= 402 \pm 73\,\mu$M, mean Fp $= 233 \pm 66\,\mu$M, and mean Fp redox ratio $= 0.37 \pm 0.08$.

Figure 5 shows typical redox scanning images and their corresponding histograms of a normal mouse liver. The range of Fp nominal concentration

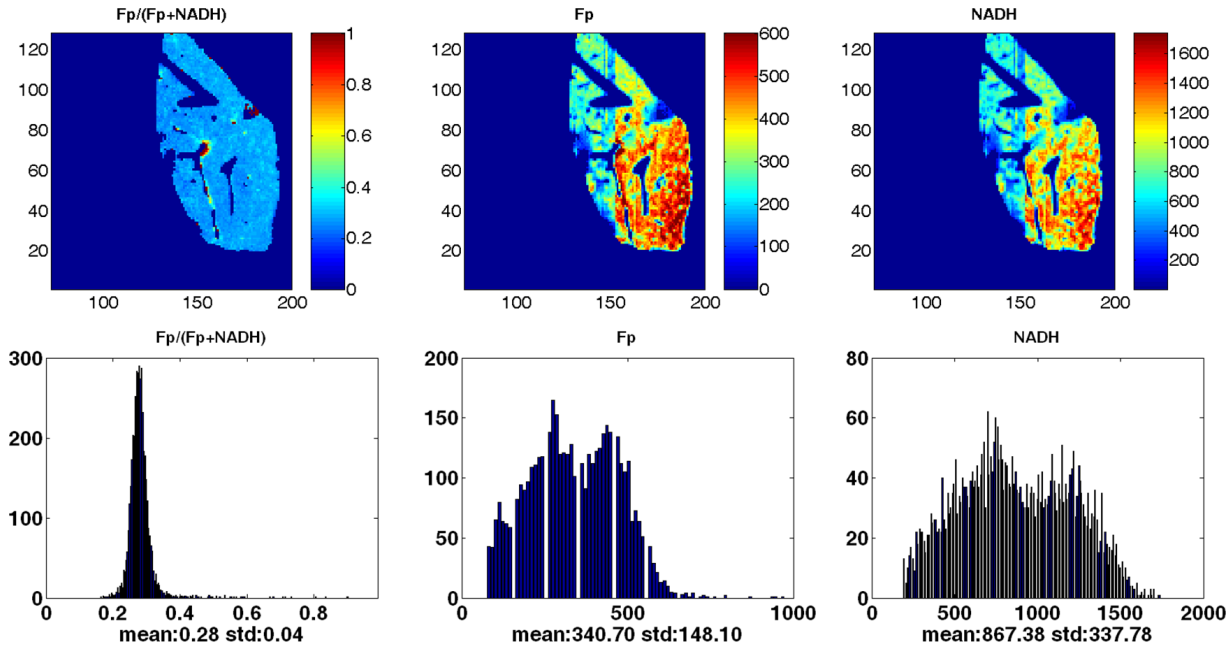

Fig. 5. Typical redox scanning images and their corresponding histograms of a normal mouse liver. Matrix size: 128 × 128, resolution 100 × 100 μm^2. The color bars in the top center and right images represent Fp and NADH concentrations in μM in the tissue. The histograms delineate the Fp redox ratio and Fp and NADH concentration distribution in the scanned section of mouse liver tissue. The mean value and the standard deviation are also displayed in each histogram. The standards were placed relatively far away from this organ and were omitted when constructing the images in order to show the tissue section.

was 100–700 μM, averaging 341 ± 148 μM whereas NADH distributed between 240 and 1,700 μM with an overall average of 867 ± 338 μM. Both NADH and Fp histograms show a bimodal distribution and both images indicated some level of difference between the left and the right section of the tissue. However, the Fp redox ratio shows a uniform distribution with Fp/(Fp + NADH) = 0.28 ± 0.04 and a narrow single modal histogram (FWHM = ∼0.04).

Figure 6 displays typical redox scanning images and their corresponding histograms of a normal mouse spleen. The Fp nominal concentration ranged 80–400 μM, averaging 188 ± 81 μM and NADH distributed between 90 and 520 μM with an overall average of 274 ± 102 μM. The Fp redox ratio, Fp/(Fp + NADH) = 0.41 ± 0.06 with a wide single modal histogram having FWHM of about 0.2, indicative of relatively high heterogeneity of the mitochondrial redox state in the spleen tissue section.

4. Discussion

This study has demonstrated a useful and effective calibration method using snap-frozen solution standards to quantitatively determine the redox states of tissue samples. The slope ratio of the NADH and Fp calibration curves is associated with instrument settings such as the set of filters, the type of PMT, the lamp, and the fiber-optic probe used. Narrow pass optical filters with a high out-of-band rejection O.D. were the key to low signal background and correct calibration. In our previous study,[28] we showed that certain UV or blue light gelatin filters may have red light leakage, which causes a high background signal, affecting the slope of the calibration curve and the slope ratio. In addition, different types of PMTs have differential sensitivity in blue or red band, and may result in a difference in the slope ratio of the two calibration curves. The type of fiber optic is another contributing factor to the slope ratio. Because light transmission is wavelength-dependent, glass fiber bundle transmits UV and red light differentially. The fiber-optical bundle using quartz (fused silica) improved UV light intensity by a factor of about 4 compared to the regular glass fiber-optical probe. Although applying higher voltage to the PMT increases slope of each calibration curve, such increase occurs to the two fluorophores in the same manner, resulting in a stable slope ratio (with a variation of ∼3%).

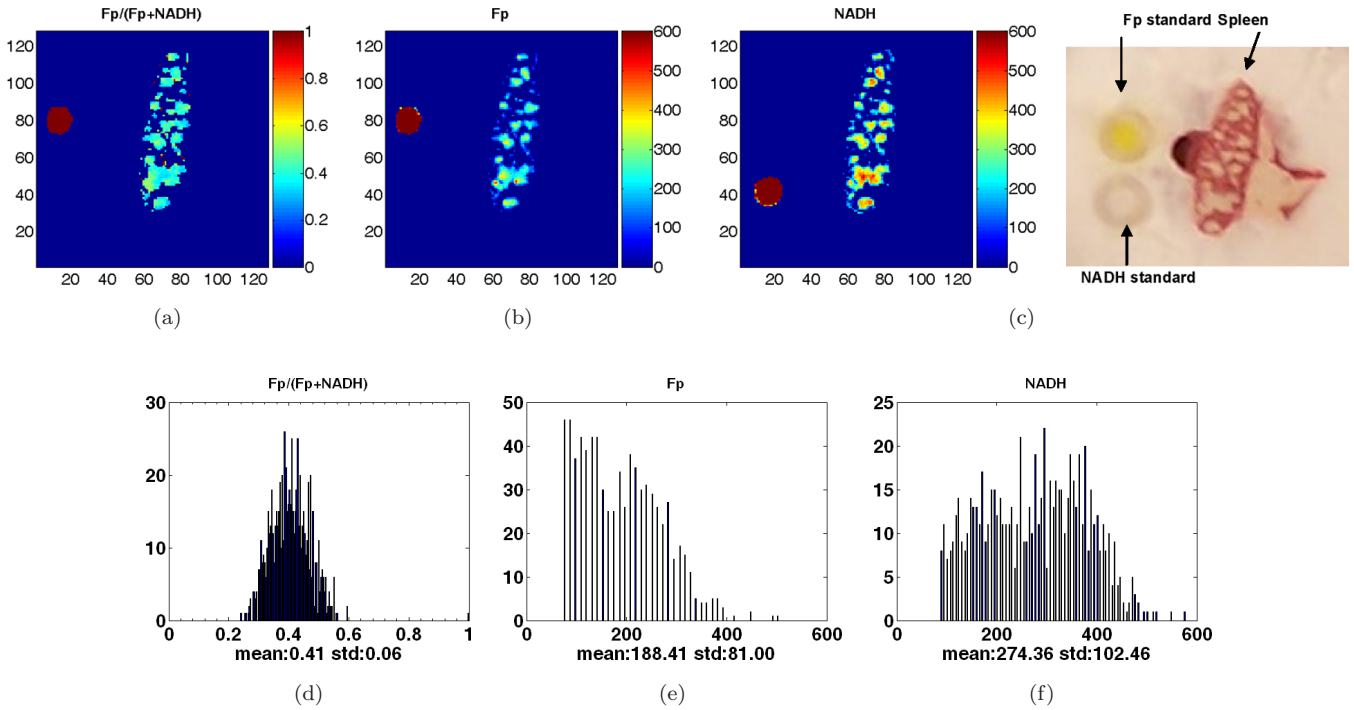

Fig. 6. Typical redox scanning images and their corresponding histograms of a mouse spleen. Matrix size 128×128, resolution $100 \times 100\,\mu m^2$. A photo of the sample of the scanned section was also displayed in the top row.

The calibration curves can also be used for calibrating the redox ratio images of the tissue samples made without reference standards. Knowing the slope ratio of NADH and Fp calibration curves enables the conversion of signal intensity-based redox ratio to concentration-based ratio, under the condition that the calibration curves and the redox images of the samples are obtained under the same instrument settings. If we define the slope ratio of NADH to Fp calibration curve as α, signal intensity-based Fp redox ratio $R_s = \mathrm{Fp}/(\mathrm{NADH} + \mathrm{Fp})$, then the concentration-based Fp redox ratio $R_c = \mathrm{Fp}/(\mathrm{NADH} \cdot \alpha^{-1} + \mathrm{Fp}) = \alpha/(\alpha - 1 + R_s^{-1})$.

In our study, the concentration of NADH stock solution was 2–3 mM and that of the standards matrix were between 0.16 and 1.3 mM. The concentration of the reference standard used for tissue samples was chosen within the linear dynamic range determined by the standards matrix. The aliquots of the stock solution were stored in a freezer of temperature at $-80°$C. The standards embedded in tissue sample were stored in liquid nitrogen. Additionally, before conducting redox scanning of a prepared sample, we shaved away the sample surface with a thickness about 100–200 μm. This shaving procedure ensures the surface is fresh and free of oxidization for fluorescence measurements. Enzymatic analysis has shown that if stored in a freezer of temperature at about $-80°$C, NADH solutions (0.4 and 40 mM) can be stored for months without any loss of activity.[29] Therefore, although we have not systematically conducted studies on the stability of the standards, we expect that our standards stored either in a freezer of $-80°$C or at liquid nitrogen temperature should be very stable with time.

Generally speaking, the relationship between tissue fluorescence and the fluorophore concentration may not be linear, and it may be better to scan a matrix of standards (of various concentrations) together with biological tissue so that the tissue fluorescence can be quantified and calibrated in the full range of the fluorophore concentration in tissue. In the present study, a linear relationship between tissue fluorescence and the fluorophore concentration was assumed, and the concentrations selected for making the reference standards in the applications fall into the linear dynamic range determined by scanning the standards matrix. Our experience indicated that one standard for each fluorophore can also serve as a reference fairly well.

An alternative is to make a mixed standard by mixing the two fluorophores (NADH and FAD) in the same solution. On one hand, mixed standard

may simplify the sample preparation by reducing the numbers of reference standards. On the other hand, there is a complexity that NADH fluorescence may be absorbed by FAD so that NADH fluorescence of the same concentration may depend on the amount of FAD in the mixed standard. This process may actually happen in tissue as well, posing a challenge for the determination of the true concentration of NADH/FAD in tissue by optical imaging method. It may be possible to design a better calibration method in the future by taking into account of this FAD re-absorption issue when using mixed standards.

The fluorophore concentrations determined for tissue samples in this study are nominal values, i.e. fluorescence differences without correction for quantum yields and hemoglobin absorption, and they may deviate from the true concentrations in tissue due to absorption by hemoglobin in red blood cells.[23] The possible difference of scattering constants between tissue and the reference standards is another source of error. Furthermore, these nominal concentrations could be over-determined since a significant portion of these fluorophores binds to proteins in tissues, and protein-bound forms exhibit stronger fluorescence than the free form in solutions,[30,31] although the NADH nominal concentration determined in this work falls within the physiological range of NADH concentration reported in literature.[32] In the future, improved calibration method of determining the fluorophore concentration in tissue could possibly be performed by using correction procedures as reviewed by Bradley and Thorniley[33] or by comparing redox scanning results with those determined by mass spectrometry in the same biological tissue sample. Nevertheless, the nominal NADH and Fp concentrations determined by solution standards can serve as a reliable reference for comparing results acquired at different time and independent of instrument settings.

By using the calibration of reference standards, this study has further demonstrated a reliable way of quantitatively imaging the redox states of typical tissue samples, i.e., a breast tumor xenograft, a normal mouse liver, and a normal mouse spleen. The breast tumor (MCF-7 line, indolent) model showed that NADH distributed in the range of 200–600 μM with an average of 402 μM, and Fp was between 100 and 450 μM with an average of 233 μM. The Fp redox ratio of the tumor sample was 0.2–0.6 with FWHM of $\sim$0.15 and an average of 0.37. There was no obvious core and rim difference, consistent with our previous results on indolent human melanoma mouse xenografts.[20–22]

The mouse liver showed that NADH was between 240 and 1,700 μM (avg. 867 μM) and Fp between 100 and 700 μM (avg. 341 μM), both having much higher overall average than that in the MCF-7 breast tumor. The mean value of Fp redox ratio was 0.28 with very narrow FWHM ($\sim$0.04). This indicates relative homogeneity of the mitochondrial redox states in the liver tissue section.

The spleen concentration was less in both NADH and Fp compared with that in the liver. Compared to liver section, it showed higher heterogeneity in the mitochondrial redox states with Fp redox ratio distributing between 0.2 and 0.58 and FWHM of 0.2. In average, the spleen section was more oxidized (average Fp redox ratio 0.41) than that of liver (average Fp redox ratio 0.28). In the spleen, the white pulps had much higher NADH and Fp than the red pulps, while the latter was hardly detected. The white pulps contain mainly B-lymphocytes and T-lymphocytes while the red pulps contain blood and reticular fibers composed of type III collagen. The two types of pulps have distinct and yet complementary functions.[34] The composition and function differences between the white and red pulps may account for the observed results in this study. More tissue samples need to be redox imaged to reliably compare the mitochondrial redox state in different organs and between normal and disease tissues.

Fluorometry is probably the only practical imaging method available for measuring NADH and Fp (FAD) in tissue. In addition to the single photon redox imaging method, two photon fluorescence imaging is another approach that can be used for measuring NADH-Fp redox state in tissue[35–39] and cell culture.[4,40] These techniques can achieve a higher resolution of submicron and certainly are appropriate and valuable for the related studies; however, resolution of 50–100 μm seems to suffice for imaging tumor sections according to our previous studies.[22] Although many studies that image NADH or FAD in tissue with single photon or two-photon fluorescence methods have been reported, not many of them have conducted measurements of both NADH and Fp simultaneously and obtained the redox ratios. Ratiometric method has the advantage of obtaining redox state independent of mitochondrial densities and cancellation or suppression of the interference of other fluorophores

or absorbers such as hemoglobin. Snap-freezing live animals or their organs to preserve the *in vivo* metabolic status was not always used for tissue sample preparation in some studies.[35,36,38] Additionally, the calibration procedure to obtain the nominal NADH and Fp concentrations in tissue was often not used in these studies. However, as demonstrated by our research experience including the study reported here, such a calibration procedure is rather useful for facilitating the comparisons among the redox images of tissue samples independent of instrument settings.

5. Concluding Remarks

In this paper, we have reported the further development of the low-temperature 3D redox scanning instrument to quantitatively determine the nominal NADH and Fp concentrations in tissue samples by a calibration procedure of using snap-frozen solution standards. The redox scanner showed a good linear dynamic range from 165 to 1,318 μM and Fp from 90 to 720 μM. The snap-frozen solution standards also served to determine the nominal concentrations of NADH and Fp in various tissue samples, such as human breast cancer mouse xenografts, a mouse liver, and a mouse spleen, demonstrating that the nominal concentrations of NADH and Fp and concentration-based redox ratios for tissue samples could be obtained quantitatively. The obtained redox images are independent of instrument settings, facilitating the comparison of images obtained at different time, with different instrument settings, and/or with different tissue samples. This redox imaging method provides a concentration-based quantitative measure of the *in vivo* mitochondrial redox state of the tissue under investigation.

Acknowledgments

This work was partially supported by the Susan G. Komen Foundation Grant KG081069 (PI: L. Z. Li), an NIH supported research resource (P41-RR02305, PI: R. Reddy), the Network of Translational Research in Optical Imaging (NTROI) at the University of Pennsylvania (U54 CA105008, PI: W. S. El-Deiry), and an NIH Grant UO1-CA105490 (PI: L. A. Chodosh). We would like to thank Mr. William Pennie for making the new UV fiber-optic probe and his consistent assistance in solving the technical issues related to the instrument. We are also grateful to Dr. Ben Stanger for providing the mice for organ harvest.

References

1. I. E. Scheffler, *Mitochondria*, John Wiley and Sons, Inc., Hoboken, New Jersey (2008).
2. A. L. Lehninger, D. L. Nelson, M. M. Cox, *Principles of Biochemistry*, Worth Publishers, New York (1993).
3. B. Chance, G. R. Williams, "Method for the localization of sites for oxidative phosphorylation," *Nature* **176**, 250–254 (1955).
4. J. V. Rocheleau, W. S. Head, D. W. Piston, "Quantitative NAD(P)H/flavoprotein autofluorescence imaging reveals metabolic mechanisms of pancreatic islet pyruvate response," *J. Biol. Chem.* **279**, 31780–31787 (2004).
5. Y. Yuan, Y. F. Li, B. D. Cameron, P. Relue, "Fluorescence anisotropy of cellular NADH as a tool to study different metabolic properties of human melanocytes and melanoma cells," *IEEE J. Sel. Top. Quant. Electron.* **13**, 1671–1679 (2007).
6. Z. Zhang, D. Blessington, H. Li, T. M. Busch, J. Glickson, Q. Luo, B. Chance, G. Zheng, "Redox ratio of mitochondria as an indicator for the response of photodynamic therapy," *J. Biomed. Opt.* **9**, 772–778 (2004).
7. A. Mayevsky, B. Chance, "Oxidation-reduction states of NADH *in vivo*: From animals to clinical use," *Mitochondrion* **7**, 330–339 (2007).
8. E. M. C. Hillman, "Optical brain imaging *in vivo*: Techniques and applications from animal to man," *J. Biomed. Opt.* **12**, 051402 (2007).
9. K. Shibuki, R. Hishida, H. Murakami, M. Kudoh, T. Kawaguchi, M. Watanabe, S. Watanabe, T. Kouuchi, R. Tanaka, "Dynamic imaging of somatosensory cortical activity in the rat visualized by flavoprotein autofluorescence," *J. Physiol. London* **549**, 919–927 (2003).
10. B. Weber, C. Burger, M. T. Wyss, G. K. von Schulthess, F. Scheffold, A. Buck, "Optical imaging of the spatiotemporal dynamics of cerebral blood flow and oxidative metabolism in the rat barrel cortex," *Eur. J. Neurosci.* **20**, 2664–2670 (2004).
11. A. Mayevsky, G. G. Rogatsky, "Mitochondrial function *in vivo* evaluated by NADH fluorescence: From animal models to human studies," *Am. J. Physiol. Cell Physiol.* **292**, C615–C640 (2007).
12. I. Hassinen, B. Chance, "Oxidation-reduction properties of the mitochondrial flavoprotein chain," *Biochem. Biophys. Res. Commun.* **31**, 895–900 (1968).
13. B. Chance, B. Schoener, R. Oshino, F. Itshak, Y. Nakase, "Oxidation-reduction ratio studies of mitochondria in freeze-trapped samples. NADH and

flavoprotein fluorescence signals," *J. Biol. Chem.* **254**, 4764–4771 (1979).
14. B. Chance, P. Cohen, F. Jobsis, B. Schoener, "Localized fluorometry of oxidation-reduction states of intracellular pyridine nucleotide in brain and kidney cortex of the anesthetized rat," *Science* **136**, 325 (1962).
15. B. Chance, N. Oshino, T. Sugano, A. Mayevsky, "Basic principles of tissue oxygen determination from mitochondrial signals," *Adv. Exp. Med. Biol.* **37A**, 277–292 (1973).
16. B. Chance, "Optical method," *Annu. Rev. Biophys. Biophys. Chem.* **20**, 1–28 (1991).
17. R. Banerjee, *Redox Biochemistry*, John Wiley and Sons, Hoboken, New Jersey (2008).
18. M. R. Hayden, J. R. Sowers, "Redox imbalance in diabetes," *Antioxid. Redox Signal.* **9**, 865–867 (2007).
19. Y. Ido, "Pyridine nucleotide redox abnormalities in diabetes," *Antioxid. Redox Signal.* **9**, 931–942 (2007).
20. H. N. Xu, R. Zhou, S. Nioka, B. Chance, J. D. Glickson, L. Z. Li, "Histological basis of MR/optical imaging of human melanoma mouse xenografts spanning a range of metastatic potentials," *Adv. Exp. Med. Biol.* **645**, 247–253 (2009).
21. L. Z. Li, R. Zhou, T. Zhong, L. Moon, E. J. Kim, H. Qiao, S. Pickup, M. J. Hendrix, D. Leeper, B. Chance, J. D. Glickson, "Predicting melanoma metastatic potential by optical and magnetic resonance imaging," *Adv. Exp. Med. Biol.* **599**, 67–78 (2007).
22. L. Z. Li, R. Zhou, H. N. Xu, L. Moon, T. Zhong, E. J. Kim, H. Qiao, R. Reddy, D. Leeper, B. Chance, J. D. Glickson, "Quantitative magnetic resonance and optical imaging biomarkers of melanoma metastatic potential," *Proc. Natl. Acad. Sci. USA* **106**, 6608–6613 (2009).
23. B. Chance, B. Schoener, R. Oshino, F. Itshak, Y. Nakase, "Oxidation-reduction ratio studies of mitochondria in freeze-trapped samples. NADH and flavoprotein fluorescence signals," *J. Biol. Chem.* **254**, 4764–4771 (1979).
24. B. Quistorff, J. C. Haselgrove, B. Chance, "High spatial resolution readout of 3D metabolic organ structure: An automated, low-temperature redox ratio-scanning instrument," *Anal. Biochem.* **148**, 389–400 (1985).
25. Y. Gu, Z. Qian, J. Chen, D. Blessington, N. Ramanujam, B. Chance, "High-resolution three-dimensional scanning optical image system for intrinsic and extrinsic contrast agents in tissue," *Revi. Sci. Instrum.* **73**, 172–178 (2002).
26. L. Z. Li, H. N. Xu, M. Ranji, S. Nioka, B. Chance, "Mitochondrial redox imaging for cancer diagnostic and therapeutic studies," *J. Innov. Opt. Health Sci.*, **2**, 325–341 (2009).
27. M. Ranji, S. Nioka, H. N. Xu, B. Wu, L. Z. Li, D. L. Jaggard, B. Chance, "Fluorescent images of mitochondrial redox states in *in situ* mouse hypoxic ischemic intestines," *J. Innov. Opt. Health Sci.* **2**, 365–374 (2009).
28. H. N. Xu, B. Wu, S. Nioka, B. Chance, L. Z. Li, Calibration of redox scanning for tissue samples, *Biomedical Optics* 71742F (SPIE, San Jose, CA (2009)).
29. J. V. Passonneau, O. H. Lowry, *Enzymatic Analysis: A Practical Guide*, Humana Press, Totowa, NJ (1993).
30. Y. Avi-Dor, J. M. Olson, M. D. Doherty, N. O. Kaplan, "Fluorescence of pyridine nucleotides in mitochondria," *J. Biol. Chem.* **237**, 2377–2383 (1962).
31. M. Wakita, G. Nishimura, M. Tamura, "Some characteristics of the fluorescence lifetime of reduced pyridine nucleotides in isolated mitochondria, isolated hepatocytes, and perfused rat liver *in situ*," *J. Biochem.* **118**, 1151–1160 (1995).
32. A. K. Ghosh, D. Finegold, W. White, K. Zawalich, F. M. Matschinsky, "Quantitative histochemical resolution of the oxidation-reduction and phosphate potentials within the simple hepatic acinus," *J. Biol. Chem.* **257**, 5476–5481 (1982).
33. R. S. Bradley, M. S. Thorniley, "A review of attenuation correction techniques for tissue fluorescence," *J. R. Soc. Interface* **3**, 1–13 (2006).
34. P. Balogh, G. Horvath, A. K. Szakal, "Immunoarchitecture of distinct reticular fibroblastic domains in the white pulp of mouse spleen," *J. Histochem. Cytochem.* **52**, 1287–1298 (2004).
35. S. Zhuo, J. Chen, T. Luo, X. Jiang, S. Xie, R. Chen, "Two-layered multiphoton microscopic imaging of cervical tissue," *Lasers Med. Sci.* **24**, 359–363 (2009).
36. L. M. Tiede, S. M. Rocha-Sanchez, R. Hallworth, M. G. Nichols, K. Beisel, "Determination of hair cell metabolic state in isolated cochlear preparations by two-photon microscopy," *J. Biomed. Opt.* **12**, 021004 (2007).
37. M. C. Skala, K. M. Riching, A. Gendron-Fitzpatrick, J. Eickhoff, K. W. Eliceiri, J. G. White, N. Ramanujam, "*In vivo* multiphoton microscopy of NADH and FAD redox states, fluorescence lifetimes, and cellular morphology in precancerous epithelia," *Proc. Natl. Acad. Sci. USA* **104**, 19494–19499 (2007).
38. S. Zhuo, J. Chen, N. Cao, X. Jiang, S. Xie, S. Xiong, "Imaging collagen remodeling and sensing transplanted autologous fibroblast metabolism in mouse dermis using multimode nonlinear optical imaging," *Phys. Med. Biol.* **53**, 3317–3325 (2008).

39. J. G. Lyubovitsky, J. A. Spencer, T. B. Krasieva, B. Andersen, B. J. Tromberg, "Imaging corneal pathology in a transgenic mouse model using nonlinear microscopy," *J. Biomed. Opt.* **11**, 014013 (2006).

40. S. Huang, A. A. Heikal, W. W. Webb, "Two-photon fluorescence spectroscopy and microscopy of NAD(P)H and flavoprotein," *Biophys. J.* **82**, 2811–2825 (2002).